Measurement of the ζ-potential in nanofluidic devices

Bachelor Thesis at the Institute of Physics of the University of Zurich

Kevin Kramer

September 13, 2014

Nanofluidic devices and electrostatic traps embedded therein have been shown to allow for size and charge measurements of individual nanoscopic objects [1]. In order to carry out actual measurements this way, the nanodevices have to be fully characterized. While the geometry is given to great precision through fabrication, the shear plane potential ζ remains an unknown parameter. Other present and future applications of micro- and nanofluidic devices also depend on knowing ζ [2][3]. Here, we present a measurement of the ζ-potential of silica devices by measuring the velocity of the electroosmotic flow induced by applying an external potential to a solution-filled device. The flow velocity is measured by using fluorescence microscopy to detect tracer particles inside the nanochannels. Image correlation techniques are used to determine the velocity of these particles, and from the relation between the flow velocity and the applied electric field strength, the value of ζ can be found. This method can principally be used to determine the ζ-potential of nanodevices of different materials.

1 Introduction

Micro- and nanofluidic devices can nowadays be fabricated with great geometrical precision. This allows for a number of applications in the fields of physical chemistry, microbiology, life sciences and others. Examples of applications include the study of voltage driven transport mechanisms (electroosmosis), capillary effects, separation of ions and biomolecules, single molecule analysis and nanofluidic electronics [2]. All of these fields depend to some extent on an understanding of the ζ-potential of the devices.

Two major methods exist for the measurement of ζ in a channel: measurement of the electroosmotic mobility or measurement of the streaming potential. The former is based on applying an external electric field to a nanochannel system and measuring the induced electroosmotic flow, while in the latter one measures electrical perturbations that result from double layer ions (cf. section 2) being transported by pressure-driven flow [3]. Here, the ζ-potential will be determined by a measurement of electroosmotic mobility.

We will start by looking at the physics of nanofluidic systems and derive the equations that allow the detemination of the ζ-potential. After that, we will discuss the principle of image correlation and its implementation in the case at hand. Finally, the experimental procedure is described and the results are presented, analyzed and discussed.

2 Analysis

The nanofluidic system at hand consists of silica channels of heights between $100\,\mathrm{nm}$ and $300\,\mathrm{nm}$ and significantly larger scales in the other dimensions. If filled with an aqueous solution, the ionic distribution forms the so called electrical double layer (EDL) (cf. figure 1). An external electric field is applied along the channels which results in a plug-flow as the EDL-ions are dragged towards the respective electrode. For a slightly charged particle, the movement is defined by two forces acting on it: the electrostatic attraction/ repulsion in the field and the drag exerted on it by the surrounding fluid molecules.

The physics required in describing this system is hydrodynamics of incompressible fluids, the Debye-Hückel theory of electrolyte solutions and the formulation of the electrical double layer. In this section we will analyze the problem of electroosmotic flow in nanodevices very similarly to [4].

2.1 Electrical Double Layer Formulation

Hydrodynamics of incompressible fluids is governed by the Navier-Stokes equation:

$$\rho\left(\frac{\partial \mathbf{v}}{\partial t} + \mathbf{v}\cdot\nabla\mathbf{v}\right) = -\nabla p + \eta\nabla^2\mathbf{v} + \mathbf{F}\,. \tag{1}$$

Where:

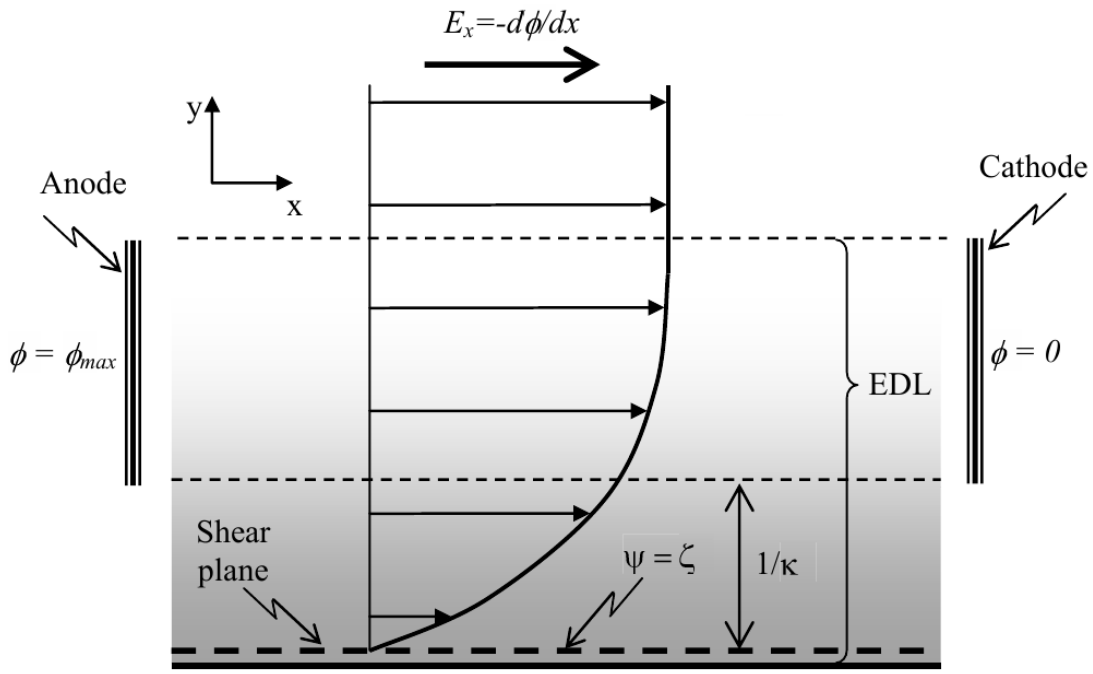

Figure 1: *The electrical double layer.*

ρ	:	liquid density
$\mathbf{v}$	:	fluid velocity
p	:	pressure field
η	:	liquid viscosity
$\mathbf{F}$	:	other body forces

In the case of electroosmotic flow the only body force is $\mathbf{F} = \rho_e \nabla V$ with the electric charge density ρ_e and the electric potential V. While the assumption of incompressibility is well satisfied, we will also assume the viscosity to be constant, which might not hold as well, due to the temperature dependence of the viscosity and the fact that there might be a significant amount of Joule heating when applying the external potential [5].

Since we are working in the strongly laminar regime, the left hand side terms of equation 1 can be neglected. Also, the pressure gradient is zero and we assume no relevant x and z dependence of $\mathbf{v}$. Equation 1 can then be simplified to:

$$\eta \frac{\mathrm{d}^2 v_x}{\mathrm{d}y^2} = \rho_e \cdot E_x \,, \tag{2}$$

where $E_x = -\nabla V$ is the electric field.

For $\rho_e = 0$, which would be the case in vacuum or if the ions were distributed uniformly in the solution, this would reduce to the Laplace equation. A non-zero charge density, however, results from the dissociation or adsorption of ions at the wall of the nanochannel. In the case of silica glass surfaces, this is mainly due to dissociation of terminal silanol groups [6]:

$$\mathrm{SiOH} \rightleftharpoons \mathrm{SiO^-} + \mathrm{H^+} \,. \tag{3}$$

The charge density drops off with increasing distance from the wall until it reaches a constant value in the ionic bulk (figure (1)). The region of varying density is referred to as the *electrical double layer*.

The Poisson equation relates the charge density to the EDL potential ψ:

$$\varepsilon_r \varepsilon_0 \Delta\psi = \rho_e \; . \tag{4}$$

The distribution of ions of type i near the surface can be described by the Boltzmann distribution:

$$n_i = n_i^0 \text{exp}\left(\frac{-z_i e\psi}{k_b T}\right) \tag{5}$$

with number density n_i, valence z_i, Temperature T and Boltzmann constant k_b. Here we have assumed that the only work done by bringing a ion of charge $z_i e$ to a point with electric field strength ψ is the electrical work done by the ion as a point charge.

The total charge density is then given by the sum over the charge distributions created by each type of ion:

$$\rho_e = \sum_i z_i e n_i \; . \tag{6}$$

Assuming a symmetrical two species solution ($i = 1, 2; z_1 = -z_2 \equiv z; n_1^0 = n_2^0 \equiv n_0$), this gives:

$$\rho_e = |z| e n_0 \left(\text{exp}\left(\frac{-ze\psi}{k_b T}\right) - \text{exp}\left(\frac{ze\psi}{k_b T}\right)\right) = 2|z|en_0 \text{sinh}\left(\frac{-ze\psi}{k_b T}\right) \; . \tag{7}$$

This can be inserted back into the Poisson equation (4):

$$\varepsilon_r \varepsilon_0 \Delta\psi - 2|z|en_0 \text{sinh}\left(\frac{-ze\psi}{k_b T}\right) = 0 \tag{8}$$

which can be linearized in the second term to yield the so called Debye-Hückel approximation:

$$\Delta\psi - \kappa^2\psi = 0 \; ; \quad \kappa = \sqrt{\frac{2z^2 e^2 n_0}{\varepsilon_r \varepsilon_0 k_b T}} \tag{9}$$

with the inverse Debye length κ. The requirement for the linearization to be justified is that the argument of the hyperbolic sine is smaller than unity:

$$\frac{ze\psi}{k_b T} \ll 1 \quad \text{or} \quad ze\psi \ll k_b T \, . \tag{10}$$

In our case, it is safe to assume that the EDL-potential varies only perpendicular to the channel surface $\psi = \psi(y)$, thus the Laplace operator in equation 9 becomes a second derivative with respect to y.

2.2 Channel Velocity

The function

$$\psi(y) = \zeta \left(e^{-\kappa y} + e^{-\kappa(h-y)}\right) = 2\,\zeta\, e^{-\kappa h/2} \cosh\left(\kappa(y - h/2)\right) \tag{11}$$

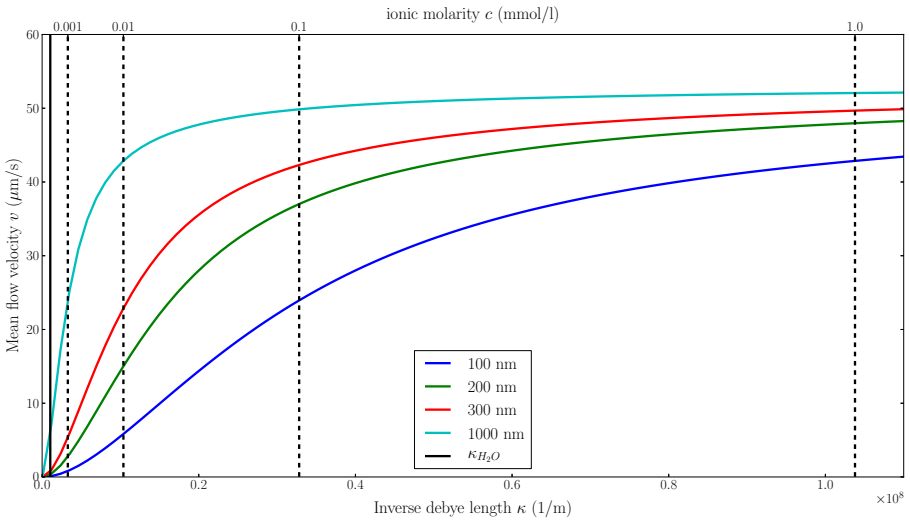

Figure 2: *Plot of mean velocity v_{mean} versus inverse Debye-length κ as in equation (15) for 4 different channel heights and electric field E = 1500 V/m. The upper x-axis gives selected values of ionic strengths corresponding to the respective values of κ.*

solves equation (9) for a channel of parallel plates at distance h with shear plane potential ζ. Combining this and (4) with (2) gives (

$$\frac{\mathrm{d}^2 v_x}{\mathrm{d}y^2} = -\frac{\varepsilon_r \varepsilon_0}{\eta} E_x \kappa^2 \psi \tag{12}$$

and upon integrating twice and applying the no-slip boundary condition $v_x(0) = v_x(h) = 0$ and the symmetry argument that the maximum of the profile must be in the centre of the channel $\left.\frac{\mathrm{d}v_x}{\mathrm{d}y}\right|_{h/2} = 0$:

$$v_x(y) = \frac{2\varepsilon_r \varepsilon_0 E_x}{\eta} \zeta e^{-\kappa h/2} \left[\cosh\left(\kappa h/2\right) - \cosh\big(\kappa\left(h/2 - y\right)\big) \right] . \tag{13}$$

For the maximum velocity in the centre of the channel we find:

$$v_{max} = \frac{2\varepsilon_r \varepsilon_0 E_x}{\eta} \zeta e^{-\kappa h/2} \left[\cosh(\kappa h/2) - 1 \right] , \tag{14}$$

and for the mean velocity along the channel:

$$v_{mean} = \frac{2\varepsilon_r \varepsilon_0 E_x}{\eta} \zeta e^{-\kappa h/2} \left[\cosh(\kappa h/2) - \frac{2}{\kappa h} \sinh(\kappa h/2) \right] . \tag{15}$$

These terms for the general fluid velocity do not necessarily describe the velocity of a particle in the solution. Such a particle experiences a force by the electroosmotic flow as well as an electrophoretic force according to its charge. Ideally, one would thus use an electrically neutral particle as a tracer.

As shown by [4] and [7], in the Debye-Hückel approximation the double layer potential ζ corresponds to the wall charge density:

$$\sigma = -\varepsilon_0 \varepsilon_r \kappa \zeta \, . \tag{16}$$

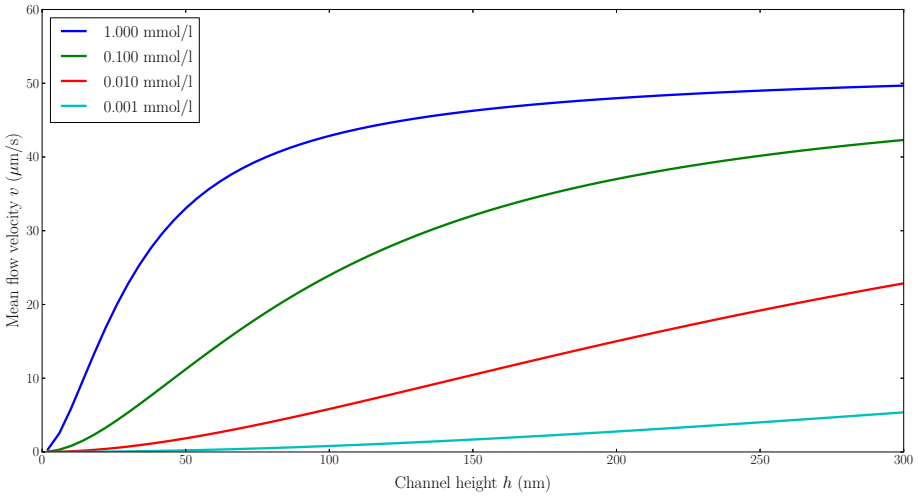

Figure 3: *Plot of mean velocity v_{mean} versus channel height h as in equation (15) for 4 different salt concentrations and electric field E =* 1500 V/m.

3 Image Correlation Code

In order to accurately determine the velocity of a particle from a `tiff` file a `python` program based on the principle of image correlation is created. Another program which simulates experimentally obtained `tiff` movies is written as well and it is used to test the functionality of the image correlation code under different conditions and to get a measure of the accuracy of said code. This knowledge is then used to set the parameters of the experiment such that the resulting movies can be analyzed properly. In the following section we will review the principle of image correlation, show how this has been implemented in our case, look at the behaviour of the code for differently parametrized simulated movies and discuss one of the biggest difficulties when it comes to analyzing experimental data with the code: the background.

3.1 Image Correlation

The cross-correlation of two functions $f(t)$ and $g(t)$ is defined by:

$$(f \star g)(t) := \int_{-\infty}^{\infty} f^*(\tau)\, g(\tau + t) d\tau \,. \tag{17}$$

Here f^* denotes the complex conjugate. This is used in signal processing to measure the similarity of the functions f and g subject to a translation t. Graphically speaking, to get the cross-correlation one slides the first function over the other and takes the integral of the product of the two at every point (cf. figure 4).

In image processing, where one usually deals with real functions of integers, the cross-correlation can be discretized to:

$$(f \star g)(n) = \sum_{i=-\infty}^{\infty} f(i)\, g(i + n) \,. \tag{18}$$

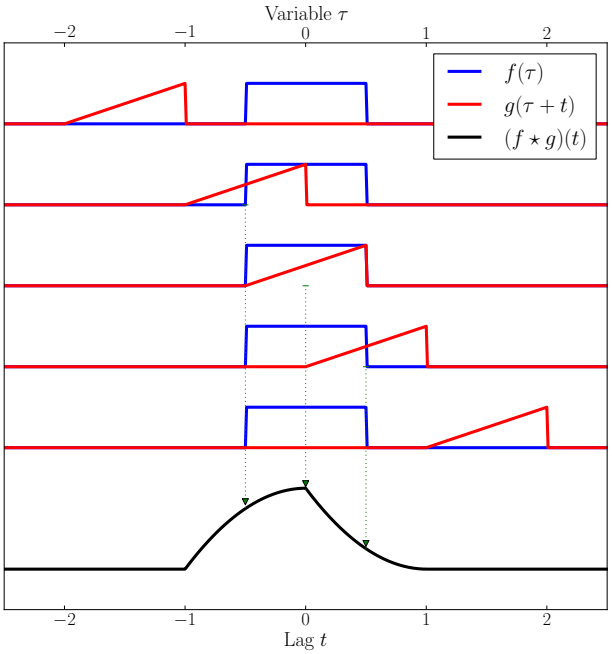

Figure 4: *Illustration of cross-correlation. The red signal slides over the blue one. The integral of the product of red and blue for each lag n is given by the black curve – the cross-correlation.*

A natural way of deciding whether two one dimensional images, i.e. arrays of integers of length N, are similar to each other is to measure the sum of the square of the differences between values in the two images. The smaller the square difference, the more they should look alike.

$$\begin{aligned} \text{Sum of square differences} &= \sum_{i=0}^{N} \left(f(i) - g(i)\right)^2 \\ &= \sum_{i=0}^{N} f^2(i) + \sum_{i=0}^{N} g^2(i) - 2\sum_{i=0}^{N} f(i)\, g(i) \end{aligned} \tag{19}$$

The first and the second term in (19) depend only on the first or second image respectively. The third term, however, depends on both images. In order to minimize the sum of square differences, one has to maximize this third term. If we translate g by a number $n \in 0, \pm 1, \pm 2, \ldots, \pm N \quad (g(i) \to g(i+n))$ we can identify this term with the cross-correlation $f \star g$. Thus, by calculating the cross-correlation of two images one can not only get a measure for their similarity, but also find how much the images are shifted from each other by finding the maximum of $(f \star g)(n)$.

In other words, if we slide one image over the other, the integral of the product will get large if the peaks and troughs of both images overlap.

Note that in the second term, after doing the substitution $(g(i) \to g(i+n))$ the variable $n + i$ may exceed the function's domain. Thus, the term depends on how this case is treated. The simplest method to deal with this is to pad with zeros,

i.e. define $g(i) = 0$ for $i < 0$ or $i > N$. Another way would be to pad with the respective values of g at the edges. Slightly more elaborately, one can also pad with decreasing values, converging to zero. In the case at hand, zero padding is used as the difference in the result is negligible here.

The principles explained in this section can easily be generalized for the two dimensional case [8].

3.2 Implementation

The principle of image correlation is implemented through `python`'s built-in `correlate()` function provided by the `numpy` module. A `tiff` file of $N \times M$ pixels and f frames gets collapsed into an $N \times f$ array by summing over each row. In this set of f one dimensional images, every frame gets correlated with its direct neighbour. The average is taken over the $f - 1$ correlation coefficient arrays. Then, three approaches are made to find the peak of the cross-correlation. The most naïve way is to just take the maximum. Since the distribution is discretized, one can achieve a slightly more precise result by fitting a gaussian at the data and taking its mean value μ for the maximum. While this works in ideal cases, background issues and coincidental correlations tend to create additional peaks that may outwheigh the relevant one. Thus, a more involved, semi-automatic way of identifying peaks is applied (cf. section 5.2.1).

This procedure can be repeated with correlation coefficients obtained by correlating each frame f with frame $f + 2$ or $f + 3$. This way, one gets up to three data points to apply a linear fit on (including point $(0, 0)$) and obtain a better average for the actual shift.

3.3 Code characterization

In order to measure the performance and accuracy of the image correlation code, `tiff` files are simulated and run through it. These simulated videos contain a certain number of particles moving at a certain velocity through a channel. They implement Brownian motion in three spatial dimensions, background noise, constant backgrounds and the microscope's point-spread function for particles – all adjustable and set to match the real experimental situation as closely as possible.

The main parameters the code is tested against are the **number of particles** nPr that corresponds to the particle density, the **noise to signal ratio** nts[1] and the **particle velocity** v. Two of these parameters are set to a value at which the code is known to work well while the third is varied. All other parameters remain constant. For each value of the varied parameter, 100 movies are generated and evaluated by the image correlation code. The mean difference between the resulting velocity from the code and the actual velocity in the simulated movies is taken as a measure for the code's accuracy under these conditions. Functions are fitted at the respective values and these functions are then used to calculate the uncertainty stemming from the code in actual experiments. The values for the fixed parameters are $v = 25, npr = 60, nts = 0.5$. Plots of the results can be found in figures 5, 6 and 7. A function is plotted to the respective data point (dashed lines in figures). They are used to model the error of the code. Fitting parameters for these functions can be found in the appendix (5.2).

[1] As opposed to the more conventional *signal to noise* ratio.

The results mostly confirm what is intuitively clear:

- The code works indifferently from particle velocity v, as long as it does not get too big. If the particles are moving so fast that they are only on screen for two frames or less, one can no longer follow the path of one single particle. This can be seen in figure 5 in the sudden drop around $v_{in} \approx 50$.
- If the background noise gets closer to or greater than the signal strength, the correlation code has to compare random images with the same mean values but no defined structures. This will lead to a correlation coefficients peak at zero. Thus, the code output will be zero and the difference of output to v in figure 6 approaches v quickly for $nts > 0.7$.
- If there are very few particles, the relative positions of the particles from each other change a lot in every frame due to Brownian motion. In such a situation, every lag at which two particles overlap creates a high correlation coefficient, even if the particles do not actually correspond to each other. With more particles, areas with high densities are less susceptible to moving faster or more slowly than other such areas and thus, the distances between high density areas stay the same which allows for less ambiguos correlation.

  It has to be noted that the code stops working for too high densities, as this results in correlating almost white images with each other. Testing this properly, however, proved too calculation expensive.

3.4 Background handling

For videos with a constant signal in the same spot, as it may occur if a particle gets stuck or if any other structure in the background emits light, the code breaks down if the background signal strength is similar to the one of the particles as this produces an immense peak at zero. In this case, background subtraction becomes crucial. The most intuitive way would be static background subtraction: take a frame with no particles in it and subtract it from all the other frames. Such a frame turns out to be hard to produce in experimental reality due to numerous reasons. One is left with the possibility of subtracting the frame with the fewest particles in it which leads to an improvement in most cases, but does not work universally. Additionally, the background might change over time with bleaching effects or new particles getting stuck in the region of interest.

An alternative is to avoid correlating images with many similarities by looking at their differences instead: dynamic background subtraction. Subtracting one image from the subsequent other will cancel all constant background disturbances and produces an image that - in the ideal case - has the first image in positive values and the second in the negative. Taking these positive and negative parts respectively and correlating them comes very close to correlating everything that is not constant background. It turns out that this method almost completely solves most background issues. Only for low velocities, i.e. small differences between two subsequent images, dynamic background subtraction cancels out too much of the actual signal, so static subtraction is advised in these cases.

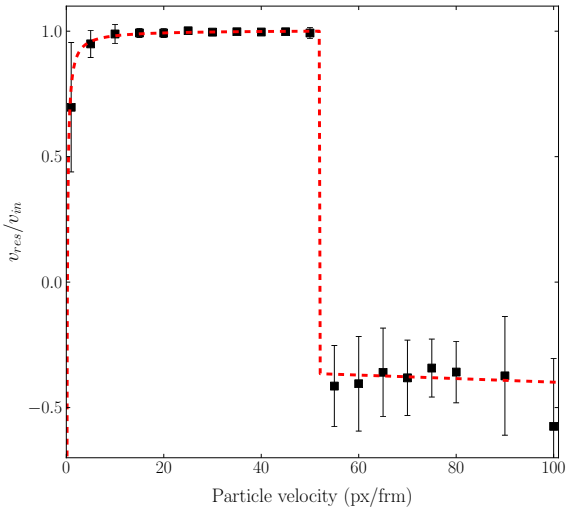

Figure 5: *Ratio of simulated velocity v_{in} and output velocity v_{res} as a function of the simulated velocity v. The dashed line is a fit of $f(x) = (a_0 + a_1 \cdot x) \cdot \text{heaviside}(a_2, x) + a_3 + a_4/x$.*

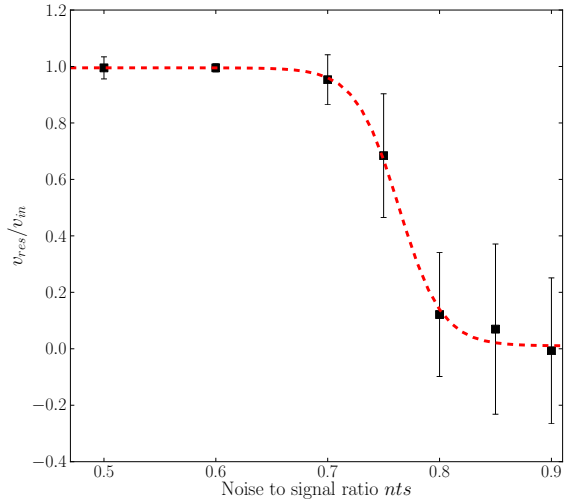

Figure 6: *Ratio of simulated velocity v_{in} and output velocity v_{res} as a function of the simulated noise to signal ratio nts. The dashed line is a fit of the heaviside approximation $f(x) = a_0 + a_1/(1 + \exp(a_2 \cdot x + a_3))$.*

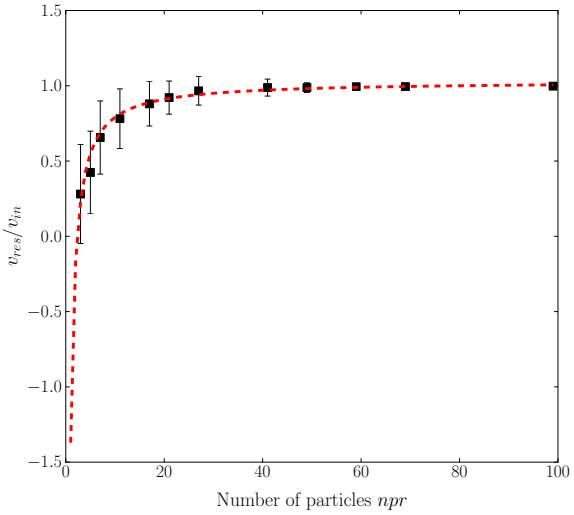

Figure 7: *Ratio of simulated velocity v_{in} and output velocity v_{res} as a function of the simulated number of particles npt. The dashed line is a fit of the function $f(x) = a_0 + a_1/x$.*

4 Experiment

As shown in section 2, the zeta potential ζ is linked to the electroosmotic flow velocity v through equations (13), (14) and (15). This allows us to experimentally determine the zeta potential of silica devices by measuring the flow velocity inside their channels while controlling all parameters, namely the inverse Debye length κ, the channel height h and the external electric field $E = V/d$ with electrode distance d and applied voltage V. Channel height and electric field are easy to control and hold constant. κ depends on the ionic concentration and the temperature (cf. eq (9)) which introduces some difficulties (see section 4.4).

A device can be loaded with a certain solution of known salt concentration by putting droplets of said solution on either side of it such that the channels get flooded. A water repellant marker is used to prevent the solution from flowing to the other side on any way other than through the channels. An electric field can then be generated by putting electrodes in the droplets on both sides and applying a potential difference between them.

In order to observe and measure the electroosmotic flow velocity, tracer particles are used. These particles are dragged along with the flow and travel through the channels. They can be observed using fluorescent microscopy. Videos from these observations can then be analyzed (cf. section 3) to determine the flow velocity.

4.1 Setup

As mentioned above, fluorescent microscopy is used to image the device and the tracer particles. For that reason, a microscope is designed and built using customary optical elements. The microscope features two lasers of different wavelengths to be used for excitation. For the experiment at hand, only one wavelength is necessary, though.

A schematic representation of the setup can be found in figure 8. The laser beams are adjusted for height and horizontal angle using silver alignment mirrors, before they are sent through two lenses for collimation ($L1, L2$). Collimation creates parallel light and allows us to increase the spot size of the beams. While the former is not really important in the case at hand, the latter is useful as we want to illuminate a great area of the probe. Optical density filters (OD) can be used to control the intensity of the incoming light. The two beams are brought together using a $50:50$ beamsplitter (BS) and another set of alignment mirrors to guarantee that the paths coincide. A lens ($L3$) is positioned in the back focal plane of the objective, such that the incident light leaves the objective parallel and thus illuminates an area of the probe, rather than being focused on one spot. A longpass dichroic mirror (D) is used to reflect the incident light into the objective and unwanted reflections thereof back towards the source and away from the detector. Meanwhile, the emitted light from the probe, which is above the dichroic's cutoff wavelength, gets transmitted and projected onto the detector with a last set of mirrors. In front of the camera tube, a longpass filter (F) is installed to get rid of excitation light that may have passed the dichroic mirror. Finally, a widefield lens ($L4$) is used to focus the image onto the camera's chip.

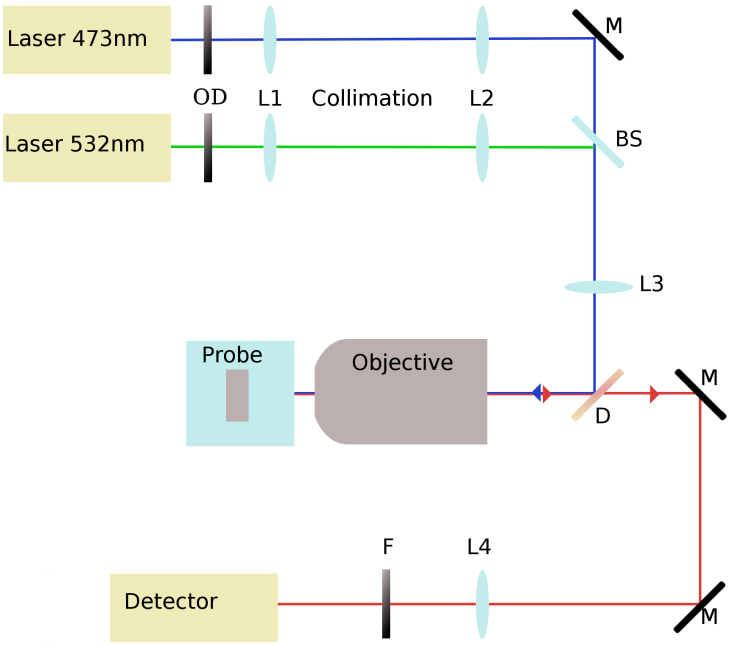

Figure 8: *Simplified scheme of the microscope. Not all mirrors (M) that were used in reality are depicted here. See text for further explanation.*

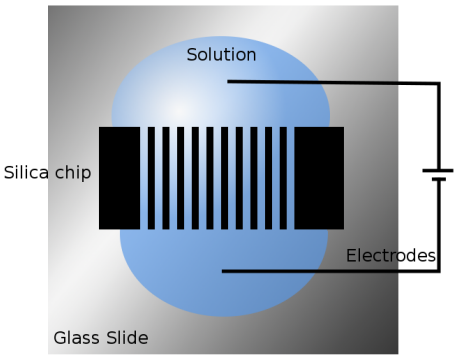

Figure 9: *Scheme of a nanofluidic device.*

4.2 Experimental Practice

The data aquisition is principally carried out as explained above. The tracer particles used are fluorescent beads of about 28 nm diameter (confer appendix for details). Solutions of these in deionized water are mixed with a known amount of sodium chloride solution to reach the desired ionic concentration. Conductivity measurements are carried out to confirm the concentration. It is verified that the conductivity of the thus prepared solution in stock remains constant over the timespan of the experiment (see also section 4.4).

Once the device has been loaded an external voltage is applied starting from 1 V and increasing in steps of 1 V. Hereby, each voltage is applied in both directions in order to avoid the build up of internal capacities and inductivities. The voltage is only applied for as short a time as needed to capture a movie (ca. 30 s) and the system is given approximately 5 minutes of no voltage after each measurement in order to relax.

Summing up, all experimental parameters are held constant – as far as possible, see section 4.4 – and only the applied voltage, and thus the electric field, is varied.

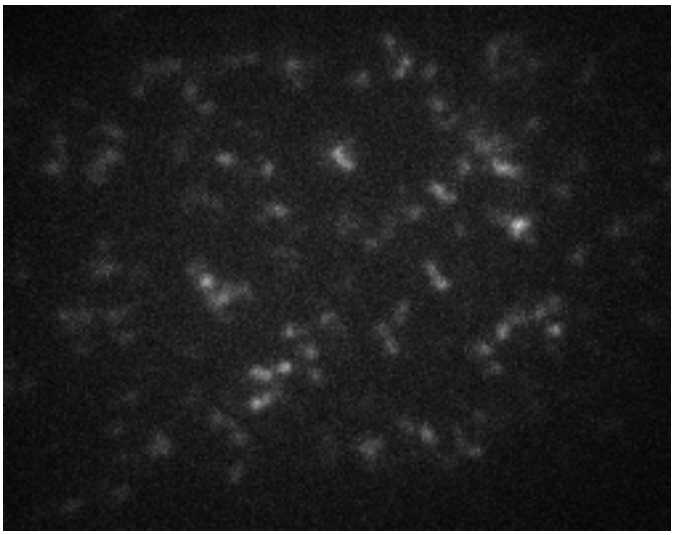

Figure 10: *A typical frame from a movie with ideal particle density (cf. section 5.1).*

4.3 Results and evaluation

The values of v in pixel per frame and V in volt are transformed to v in µm/s using

$$v_{\mu\text{m/s}} = v_{\text{px/frm}} \cdot \frac{\text{frametime}}{\text{pixelsize}}$$

and

$$E = -V/d\,.$$

The method of least squares is used to fit lines to these data points, where the points are weighted with the inverse of their uncertainties (as found by the evaluations in section 3). Plots of this can be found in figures (11), (12) & (13). With smaller channel height the measurements break down for voltages above 10 V as the beads tend to stick to each other and the walls more and more and the flow velocities – if even observable – do not seem to be correlated to the applied voltage anymore. Similar seemingly chaotic behaviour can be observed for higher ionic strengths.

From these fits, the values of the slopes v/E are extracted. The uncertainty on these values is found using a Monte-Carlo approach: The errors on the data are taken as a σ-interval for Gaussian distributions centered around the data values. 1000 sets of data are simulated this way and a line is fitted to each of these sets. The uncertainty on the original fit's slope is then taken to be the standard deviation of the slopes of the simulated data fits.

These three values of v/E are plotted against h and the function

$$\frac{v}{E}(h) = \frac{2\varepsilon_r\varepsilon_0}{\eta} e^{-\kappa h/2} \cdot \left(\cosh(\kappa h/2) - \frac{2}{\kappa h}\sinh(\kappa h/2)\right) \cdot \zeta \qquad (20)$$

where the only free parameter is the EDL potential ζ is fitted to them (cf. section 2). This is plotted in figure (14). Since an estimation of the uncertainty based on the Monte-Carlo method explained above would be quite effortful as through κ there are uncertainties on the fitting function (eq. 20) itself, Gaussian error propagation is used to find the error on ζ (see section 5).

Numerical values of quantities discussed in this section can be found in tables 1 and 2. The acquired values for the velocities as well as error propagation calculations can be found in the appendix (5).

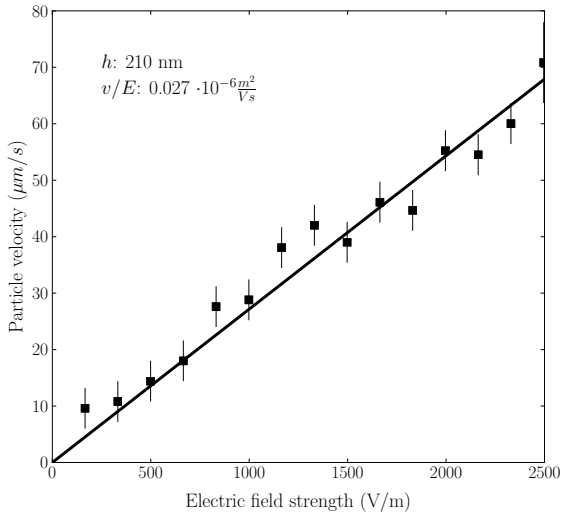

Figure 11: *Measured particle velocity v versus electric field strength E and linear fit to the data for* h=210 nm ± 5 nm.

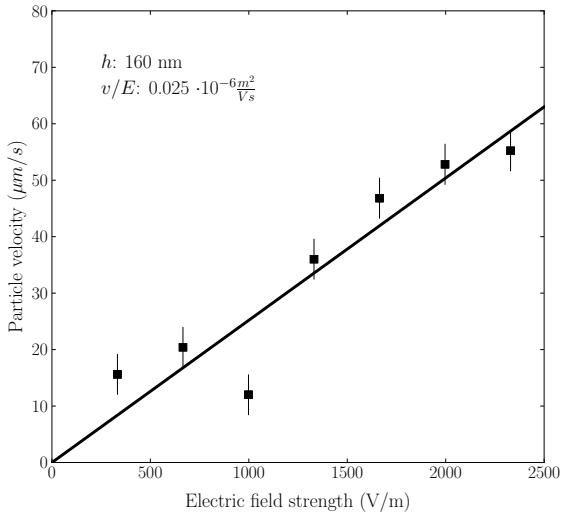

Figure 12: *Measured particle velocity v versus electric field strength E and linear fit to the data for* h=160 nm ± 5 nm.

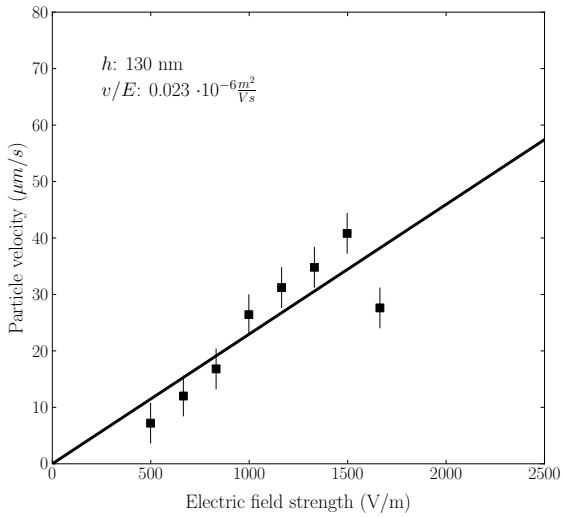

Figure 13: *Measured particle velocity v versus electric field strength E and linear fit to the data for* h=130 nm ± 5 nm.

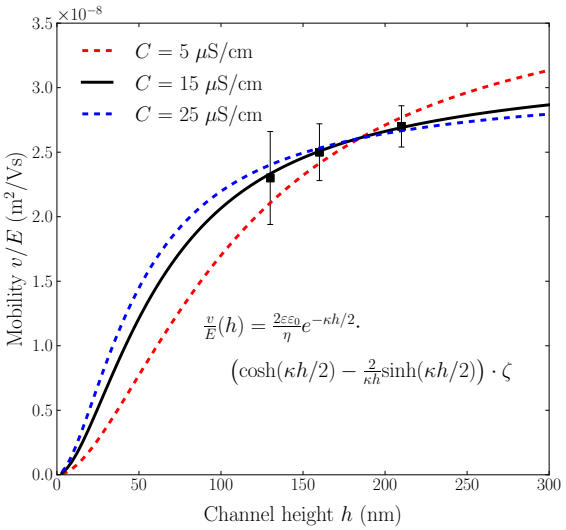

Figure 14: *Slopes v/E against channel height h with a least square fit with fit parameter ζ (black). Here, ζ evaluates to* (45 ± 9) mV. *The red and blue dotted lines give the result when assuming a conductivity C of* 5 µS/cm *and* 25 µS/cm. *The corresponding values of ζ are* 55 mV *and* 43 mV *respectively.*

Table 1: *Constants used in the calculations. The respective errors on these are negligible compared to statistical and sytematic errors of the experiment.*

Name	Symbol	Value	Unit
Dielectric constant	ε_0	$8.854187817\times10^{-12}$	F/m
Relative permittivity of water [a]	ε_r	79.2	-
Dynamic viscosity of water [b]	η	9.71×10^{-4}	Pa s
Boltzmann constant	k_b	1.3806488×10^{-23}	J/K
Elementary charge	e	$1.602176565\times10^{-19}$	C
Avogadro number	N_A	6.02214129×10^{23}	1/mol
Molar mass of NaCl	m_m	58.44	g/mol
Density of NaCl	ρ_{NaCl}	2165	g/cm^3
Conversion factor for NaCl	K	0.47	-
Valency of NaCl	z	1	-

[a] At T = 296 K, according to [9].
[b] At T = 296 K, according to [10].

Table 2: *Measured parameters with uncertainties.*

Name	Symbol	Value	Error	Unit
Pixelsize	pixelsize	122	1	µm/pixel
Exposure + Lagtime	frametime	0.102	0.001	frames/second
Temperature	T	296	1	K
Conductivity	C	15	2	µS/cm
Salt concentration[a]	c	261	30	µmol/l
Inverse Debye length	κ	53.1	3.5	µm^{-1}
Electrode distance	d	6.01	0.05	mm
Channel height	h	130, 160 & 210	5	nm
Applied external voltage	V	1 to 15 [b]	0.01	V

[a] Calculated from conductivity C.
[b] For h=130 nm V ranges from 1 V to 10 V.

The result for the double layer potential is:

$$\boxed{\zeta = (45 \pm 9)\,\text{mV}}. \tag{21}$$

With equation (16 this gives the value for the wall charge density:

$$\boxed{\sigma = (-1.7 \pm 0.4)\,\text{mC/m}^2 = (-1.1 \pm 0.2) \times 10^5\, e/\mu\text{m}^2} \tag{22}$$

4.4 Discussion

While the resulting value for ζ lies within the expected range compared to estimations based on calculations ([7]) and the data fits the proposed theory well, there are significant sources of uncertainties that shall be addressed in this section.

4.4.1 Debye-Hückel Approximation

The product $e \cdot \zeta$ – using the result 21 – amounts to about $1.8 \times k_b T$. This means the requirement 10 for the linearization of 8 is not fulfilled. Thus, the model used for determining ζ cannot be strictly justified. As can be seen in figure 15, the relative error when performing the linearization of the sinh function in this range is around $100\,\%$. Roughly estimated, this amounts to an additional uncertainty on the final result for ζ of about $5\,\mathrm{mV}$.

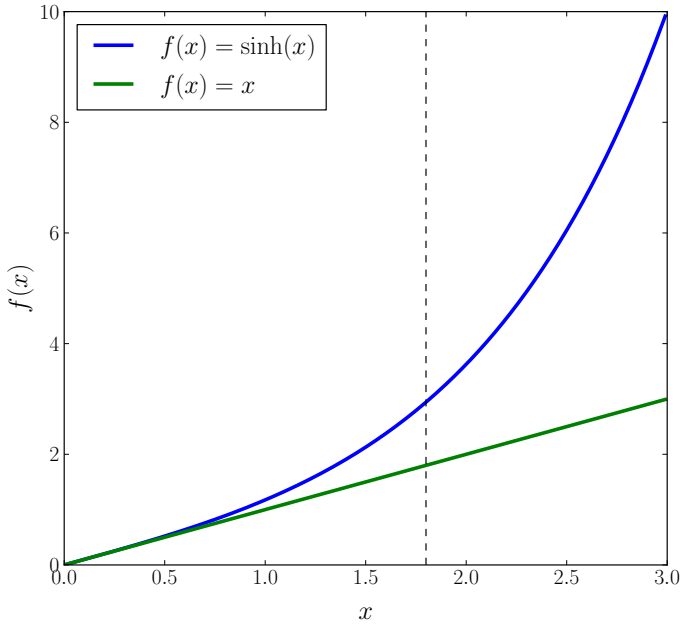

Figure 15: *Comparison of* $\sinh(x)$ *with the identity function. The dotted line indicates the value of* $e\zeta/k_b T$.

4.4.2 Inverse Debye Length κ

The value of the parameter κ comes with many possible error sources. To determine its value one has to know the ionic concentration and the temperature (equation 9).

Temperature. Other than κ, the viscosity η and the relative permettivity of water ε_r also depend on the temperature. [5] discusses the effects of joule heating due to the applied voltage on the temperature and velocity distribution of microfluidic systems. These effects appear to be relatively small for the problem at hand. Additionally, the fact that a voltage is never applied for a long timescale certainly helps to minimize possible effects of joule heating. It should be pointed out, however, that no explicit measurement of the temperature inside the device during the experiment has been conducted, so the possibility of these effects influencing the outcome cannot be discarded completely.

Concentration. While one can have relatively good control over the ionic strength of the used solution by carefully preparing a buffer of NaCl, these efforts end up in vain because of the following reasons: Once the solution is applied to a nanofluidic device, the conductivity increases as part of the Na^+- ions adhere to the silicon groups of the wall. In order to keep this effect relatively small one could prepare a

buffer of much higher concentration than what the sodium-silica interaction adds. It turns out, however, that as soon as we go to these concentrations, the experiment cannot be conducted anymore as the nanobeads do not enter the channels under these circumstances – probably due to some chemical effect. Thus, the ionic concentration has to be determined indirectly through measurements of the conductivity of the solution. This leads to a new set of problems. Conductivity measurements usually require larger volumes than were used in the experiment. The recommended volume for the used conductivity metre amounts to $200\,\mu l$ while the droplets in a typical experiment are of about $20\,\mu l$ to $30\,\mu l$ volume. The conductivity metre has been tested repeatedly for whether the results of a measurement with sufficient amounts of solution correspond to those with small volumes. It seems that the metre creates reproducable results within small errors even on these low volumes, so acquiring the conductivity of the solution before and after an experiment is possible this way.

To get the ionic concentration from the conductivity the simple relation

$$c = \frac{\rho}{m_m} \cdot K \cdot C \tag{23}$$

is used, where c is the ionic concentration, ρ the density of the dissolved substance, m_m its molar mass, K a substance specific conversion factor and C the measured conductivity. This relation specifically holds for solutions of one ionic species. In the case at hand, we treat the solution as consisting purely of NaCl in water, neglecting possible contributions from the beads or surface groups of the silicon chip that might dissolve. But even for that case, the empiric conversion factor K lies within a range of 0.47 to 0.50, introducing an uncertainty to the problem. In order to determine the appropriate value of K, the data from [11] is used and extrapolated.

The change in the final result for different values of C is shown in figure 14. As can also be seen from the analysis, the result is more stable to deviations to and at higher conductivities, rather than at low values of C.

In addition to the large uncertainty on the value of κ, the fact that the ζ-potential itself depends on the ionic strength and the pH of the used solution [3] has been neglected completely. So the resulting value of ζ is in fact just valid for the particular set of parameters used in this experiment. It would be desirable to carry out more measurements with varying ionic strength and pH in order to find ζ for a range of situations.

4.4.3 Nanobeads

The behaviour of the fluorescent beads used in the experiments is often far from ideal. In the course of experimentation, cases where the beads would not enter the device properly or not at all would occasionally come up, even if all apparent parameters would be identical to a successful situation. In the cases where the device could be loaded, sometimes significant differences in particle concentrations could be observed in different channels. This might be due to structural defects or variations in some channels. Another unexpected observation is the fact that the behaviour of the system is asymmetric with respect to the direction of the electric field. Reasonable measurements were often possible for one direction of the field: particles would flow according to the analysis and as soon as one turns the field off some backflow would occur before the system stabilized again. For the other

direction of the field, sometimes no flow occured at all, sometimes the velocity did not depend on the field strength. An explanation for this might be that even though much care had be put into conducting the experiment symmetrically, some internal capacities built up. There may also be chemical effects that play a role in this.

A major problem is the fact that the beads themselves carry a slight negative charge and are thus pulled towards the positive pole, against the overall EOF. This charge is not known precisely, so the severeness of this effect is hard to estimate. Attempts of quantizing the strength of this electrophoretic drag by comparing the measurements to an identical situation with uncharged quantum dots failed, as no useable data with quantum dots could be acquired.

One can see that there are a number of not well understood effects that reduce the reproducability of the whole experiment. It has to be pointed out that none of these effects have been accounted for in the evaluation.

5 Appendix

5.1 Methods

The imaging setup consists mainly of *Thorlabs* photonics tools. A 473 nm and a 532 nm laser source of powers 100 mW and 50 mW respectively are used for the illumination. The powers can be adjusted using optical density filters. The camera used is the EMCCD detector *Andor Luca-R* [12]. *Life technologies*' *Fluospheres*® *Carboxylate-Modified Microspheres* (F8784) are used as tracer particles. This batch has a diametre of $28\,\text{nm} \pm 4\,\text{nm}$. It turns out that a dilution of 1/1000 from stock produces a reasonable particle density. For tests with quantum dots, *Life technologies*' catalog number (Q21511MP) is used.

5.2 Data and Code

The `tiff` files used in the evaluation as well as the program codes can be found at `http://www.physik.uzh.ch/~kekram/Bachelor%20Thesis/`. The resulting velocities for these files, which are plotted in figures 11, 12 and 13, are presented in table 3. Table 4 holds the values of the fitting parameters for the functions of section 3.3.

Table 3: *Evaluated values of the velocity.*

h=210 nm		h=160 nm		h=130 nm	
Voltage (V)	Velocity (px/frm)	Voltage (V)	Velocity (px/frm)	Voltage (V)	Velocity (px/frm)
1	8	2	13	1	-[a]
2	9	4	17	2	-[a]
3	12	6	10	3	6
4	15	8	30	4	10
5	23	10	39	5	14
6	24	12	44	6	22
7	32	14	46	7	26
8	35			8	29
9	33			9	34
10	38			10	23
11	37				
12	46				
13	45				
14	50				
15	59				

[a] Code unable to produce result

Table 4: *Fitting parameters fo the functions in the code performance analysis as given in figures 5, 6 and 7.*

	a_0	a_1	a_2	a_3	a_4
Velocity v :					
	-1.33	$-7.45\text{e}{-4}$	5.20e1	1.00	$-2.27\text{e}{-1}$
Noise to signal ratio nts :					
	$9.95\text{e}{-1}$	$-9.85\text{e}{-1}$	2.60	3.97e1	
Number of particles $nprt$:					
	1.03	-2.40			

5.2.1 `findpeaks.py`

The detection of peaks in the correlation spectrum is carried out by the script `findpeaks.py` , the source code of which can be found under the link given above. The principle of the method is to detect peaks of a given function by taking its derivative and detecting zero-crossings. If the zero-crossing has negative slope, one can identify a maximum. In the implementation the derivative is approximated by the finite difference method and the result is smoothed to minimize noise. If a zero-crossing with the right slope is detected, a Gaussian is fitted to points around it in the original function and its mean is returned as the position of the maximum. This method is very successful in detecting peaks over a noisy background but also very sensitive to the various parameters (peak width, amplitude and slope thresholds, degree of smoothing), thus the dub *semi-automatic*.

5.3 Error calculation

Gaussian error propagation is used to determine the error on ζ. The uncertainty on a function $f(x_1, x_2, \ldots, x_N)$ with errors σ_i on x_i is given by the variance formula:

$$\sigma_f^2 = \sum_{i=1}^{N} \left(\frac{\partial f}{\partial x_i} \right)^2 \cdot \sigma_i^2 \,. \tag{24}$$

With $\chi = \kappa h/2$ and $\sigma_\chi = 1/2 \cdot \sqrt{(\sigma_\kappa h)^2 + (\sigma_h \kappa)^2}$ one finds:

$$\sigma_\zeta = \frac{\eta}{2\varepsilon_r \varepsilon_0} e^\chi \cdot \left(\cosh(\chi) - \frac{1}{\chi} \sinh(\chi) \right)^{-1} \cdot \sqrt{\left(\sigma_{v/E}\right)^2 + \left\{ \sigma_\chi \frac{v}{E} \cdot \left[1 - \left(\cosh(\chi) - \frac{1}{\chi} \sinh(\chi) \right)^{-1} \cdot \left(\sinh(\chi) \left(1 + \frac{1}{\chi} \right) - \frac{1}{\chi^2} \cosh(\chi) \right) \right] \right\}^2} \,. \tag{25}$$

To actually calculate this, one first needs the error on κ which is given by:

$$\sigma_\kappa = \sqrt{\frac{2z^2 e^2}{\varepsilon_0 \varepsilon_r k_b} \left(\frac{\sigma_{n_0}^2}{4T n_0} + \frac{\sigma_T^2 n_0}{4T^3} \right)} \,. \tag{26}$$

With the error on the ionic number concentration:

$$\sigma_{n_0} = N_A \frac{\rho_{\text{NaCl}}}{\sigma_m} \sqrt{\sigma_C^2 K^2 + \sigma_K^2 C^2}\,, \tag{27}$$

where $\sigma_K = 0.01$ and all other values are listed in tables 1 and 2.

Acknowledgement

I would like to thank the members of group Krishnan at the Department of Chemistry of the UZH for their patient explanations and fruitful discussions. The countless hours spent by Dr. Gašper Kokot and Francesca Ruggeri fabricating devices for my experiments are greatly appreciated. Great thanks to Prof. Madhavi Krishnan for providing this experience and for all the guidance and advice.

A special thanks to Chris Myers for organizing a monitor for me.

References

[1] N. Mojarad and M. Krishnan, *Measuring the size and charge of single nanoscale objects in solutions using an electrostatic fluidic trap*, Nature Nanotechnology 7, 448-452 (2012)

[2] P. Abgrall and N. T. Nguyen, *Nanofluidic Devices and Their Applications*, Analytic Chemistry, 2008, 80 (7), pp 2326-2341

[3] B. J. Kirby and E. F. Hasselbrink Jr., *Zeta potential of microfluidic substrates: 1. Theory, experimental techniques, and effects on separations*, Electrophoresis 2004, 25, 187-202

[4] R. J. Hunter, *Foundations of Colloid Science, Second Edition*, ISBN 987-0-19-850502-0

[5] S. Sanchéz, J. Arcos, O. Bautista, F. Méndez, *Joule heating effect on a purely electroosmotic flow of non-Newtonian fluids in a slit microchannel*, Journal of Non-Newtonian Fluid Mechanics 192 (2013) 1-9

[6] R. K. Iler, *The chemistry of Silica*, Wiley, New York, 1979

[7] S. H. Behrens and D. G. Gries, *The Charge of Glass and Silica Surfaces*, J. Chem. Phys. 115, 6716-6721 (2001)

[8] D. Jacobs, *Correlation and Convolution* `http://www.cs.umd.edu/~djacobs/CMSC426/Convolution.pdf`

[9] A. Catenaccio, Y. Daruich, C. Magallanes, *Temperature dependence of the permittivity of water*, Chemical Physics Letters 367 (2003) 669-671

[10] J. Kestin, M. Sokolov, W. A. Wakeham, *Viscosity of Liquid Water in the Range* $-8\,^{\circ}\text{C}$ *to* $150\,^{\circ}\text{C}$, J. Phys. Chem. Ref. Data, Vol. 7, No. 3, 1978

[11] EXW Foxboro, Massachusetts, *Conductivity Ordering Guide*, `http://myweb.wit.edu/sandinic/Research/conductivity%20v%20concentration.pdf`

[12] *ANDOR Luca-R User's Guide*, `http://www.lot-qd.de/files/downloads/andor/en/emccd/luca-r_Manual_Version_1.0.pdf`